LITHOS 460–461 (2023) 107397

Contents lists available at ScienceDirect

LITHOS

journal homepage: www.elsevier.com/locate/lithos

Fractional crystallization of garnet in alkali basalts at >1.8 GPa and implications for geochemical diversity of Large Igneous Provinces

M.J. Hole [a,*], J.H. Pugsley [a], D.W. Jolley [a], J.M. Millett [a,b]

[a] Department of Geology and Geophysics, University of Aberdeen, AB242UE, United Kingdom
[b] VBPR AS, Oslo, Norway

ARTICLE INFO

Keywords:
Garnet fractionation
Petrology
Pressure
Mull
Basalt
Petrogenesis

ABSTRACT

A suite of lavas from northwest Mull, British Palaeocene Igneous Province, exhibit major and trace element characteristics that are best explained by very high pressure (>1.8 GPa) crystallization of an assemblage comprising aluminous clinopyroxene (Al-Cpx) plus garnet. The resulting series of consanguineous magmas are mildly Si-undersaturated. The trace element effects of this crystallizing assemblage are manifested in increasing light rare earth element (LREE) enrichment and heavy REE (HREE) depletion with decreasing whole-rock MgO, a predictable consequence of the bulk distribution coefficient (D) of this assemblage being $>>1$ for HREE but $<<1$ for the LREE. Early crystallization of Al-Cpx and replacement of plagioclase feldspar by garnet in the crystallizing assemblage also results in increasing or near constant Al_2O_3 abundances in cotectic compositions with MgO < ~7 wt%. Garnet as opposed to plagioclase crystallization is also reflected in the incompatibility of Sr and compatibility of Y resulting in very high Sr/Y lavas (up to 100) with high Sr (~1200 ppm) and low Y contents (~12 ppm). Lavas also have high Zr/Y (up to 30). Major element constraints suggest the crystallizing assemblage comprised ~40% garnet and 60% Al-Cpx.

Magmas that fractionated at ~1.8 GPa rose to the surface without interacting with the continental crust. Immediately underlying basalts and picrites show evidence of crustal contamination and assimilated fusible portions of the crust, therefore effectively lining the plumbing system and allowing later magmas to rise to the surface without crustal contamination. A local change in tectonic regime from extension to passive appears to be linked to a change from low pressure to very high-pressure crystallization of magmas. Whilst evidence for garnet fractionation in continental flood basalts is very rare, this paper provides a characterization of its geochemical consenquences.

1. Introduction

It is well-established that some of the observed compositional diversity in continental flood basalts (CFB), and indeed basaltic magmas of all Large Igneous Provinces (LIPs), is a result of crystallization at varying pressure (e.g., Fram and Lesher, 1997; Hole, 2018; Liu and Presnall, 2000; O'Hara, 1968; Thompson, 1974; Villiger et al., 2004, 2007; Whitaker et al., 2007; Yang et al., 2023). Magmas of LIPs formed under significant thicknesses of continental or oceanic lithosphere have the potential to pause and undergo crystallization at any depth from the final pressure of melting of mantle peridotite, a proxy for the lithosphere-asthenosphere boundary (LAB; Hole and Millett, 2016; Matzen et al., 2017), to the near-surface (e.g., Herzberg and Asimow, 2015; Hole and Millett, 2016; Matzen et al., 2017; Yang et al., 2023). Laboratory melting experiments (Liu and Presnall, 2000; Milholland and Presnall, 1998; Thompson, 1974; Villiger et al., 2004, 2007; Whitaker et al., 2007; Yang et al., 1996; Yang et al., 2023) demonstrate that pressure determines the order of crystallization of the main phenocryst phases in basaltic magmas and consequently the composition of erupted lavas (Fig. 1). O'Hara (1968) showed that with increasing pressure of crystallization the liquidus field of olivine (Ol) contracted and the field for clinopyroxene (Cpx) crystallization expanded at the expense of olivine. Additionally, the crystallization of plagioclase feldspar (Pl) occurs after Cpx at pressures > ~ 0.8 GPa but before Cpx at lower pressures (e.g., Hole, 2018; Nevaskil et al., 2004; Villiger et al., 2004; Whitaker et al., 2007). This means that at near-surface pressures the order of crystallization in a basaltic magma is Ol → Pl → Cpx whereas at 1 GPa the sequence is Ol → Cpx → Pl. Clinopyroxene becomes more aluminous

* Corresponding author.
E-mail address: m.j.hole@abdn.ac.uk (M.J. Hole).

https://doi.org/10.1016/j.lithos.2023.107397
Received 28 July 2023; Received in revised form 9 October 2023; Accepted 13 October 2023
Available online 19 October 2023

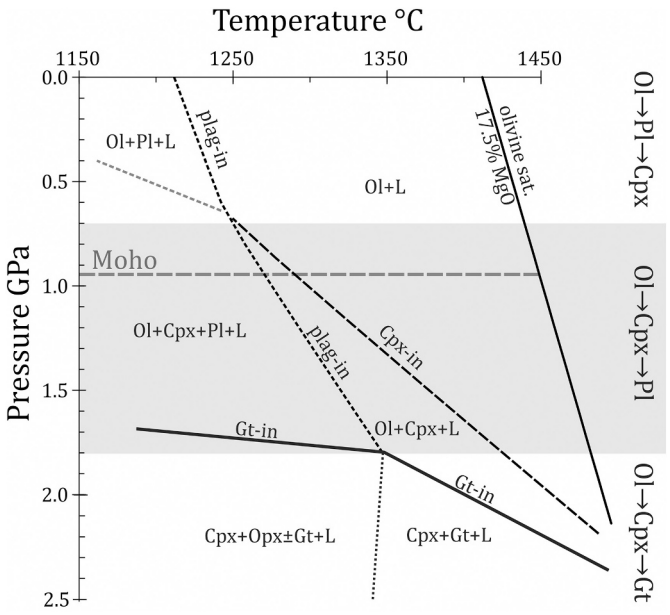

Fig. 1. a) Schematic representation of the pressure, temperature and composition relationships for the crystallization of a typical BPIP mildly alkaline magma after Hole (2018). The approximate fields of garnet stability are taken from the melting experiments of Thompson (1974) on Skye basalt SK971. The olivine saturation curve was calculated using the method of Sugarawa (2000). The order of crystallization of olivine (Ol), plagioclase (Pl), clinopyroxene (Cpx) and garnet (Gt) is indicated on the right-hand axis. The grey shaded region represents the P-T conditions where the order of crystallization is likely to be Ol → Cpx → Pl. The horizontal grey pecked line is the approximate depth to the Moho beneath the BPIP.

with increasing pressure, and the proportion of the CaTs component (calcium Tschermakite, $CaAlAlSiO_6$; calculated using the method of Putirka, 2008) increases from negligible at 1 atm to ~5% at 1GPa (Liu and Presnall, 2000; Villiger et al., 2004; Whitaker et al., 2007).

At pressures >1.8 GPa garnet is likely to replace plagioclase feldspar on the liquidus of basaltic and intermediate compositions (Bernstein, 1994; Liu and Presnall, 2000; Milholland and Presnall, 1998; Thompson, 1974; Yang et al., 2023). Indeed, Yang et al. (2023) showed near-primary melts of mantle peridotite at 3 GPa may precipitate large amounts of clinopyroxene and garnet, in approximately equal proportions, with decreasing temperature from 1350 to 1200 °C. They also argued that primary magmas to Hawaiian tholeiites experienced crystallization of clinopyroxene and garnet in magma chambers at the base of the lithosphere (~3 GPa) followed by re-equilibration with harzburgite when passing through lithospheric mantle at <2 GPa. Additionally, Bernstein (1994) appealed to garnet fractionation at high pressures (40–50 km; ~1.5 GPa) to explain variable Zr/Y in Faroes Island basaltic magmas, a proposal that was refuted by Kerr and Thompson (1995) in favour of Zr/Y being controlled by early clinopyroxene fractionation.

A role for the fractional crystallization of garnet at ~1.8 GPa was proposed by Thompson (1982) to explain the origin of a suite of 'Low Y mugearites' from the Isle of Mull in the British Palaeocene Igneous Province (BPIP) which itself forms part of the North Atlantic Igneous Province (NAIP). Kerr and Thompson (1995) argued that a positive covariation between MgO and Y in these lavas was the result of garnet fractionation "deep within the lithosphere" and resulted in the formation of mugearites (~3 wt% MgO) which exhibit anomalously low Y contents (~14 ppm), significant LREE (light rare earth element) enrichment (La ~25 ppm) and HREE (heavy rare earth element) depletion (Yb ~ 0.6 ppm), with chondrite-normalized La/Yb ($[La/Yb]_N$), ~32. The strong fractionation of LREE relative to HREE was considered by Kerr and Thompson (1995) to be the result of the compatibility of HREE with respect to garnet, whilst maintaining the incompatibility of the LREE. However, no detailed systematic study of the petrological consequences of garnet fractionation currently exists and evidence for the role for garnet fractionation in the generation of LIPs remains speculative.

In this paper we present new major and trace element geochemical data on the 'Low Y mugearites' and associated basalts and hawaiites of north-west Mull and use these data to examine the role of garnet fractionation in the petrogenesis of the lavas. We place the low Y lavas in a stratigraphical context and show that they are part of a fractionation series from ~8.0 to 3.5 wt% MgO, the major and trace element characteristics of which can be only logically explained by fractional crystallization of an assemblage of garnet + aluminous clinopyroxene which must have occurred at >1.8 GPa.

2. The north-west Mull lava pile

The Mull lava field comprised three main stratigraphical units; Staffa Lava Formation (oldest; SLF), Mull Plateau Lava Formation (MPLF) and the Central Mull Formation (youngest; Williamson and Bell, 2012). The age of the lava pile is the subject of debate (see Jolley et al., 2021 for a full discussion) but most magmatism is likely to have taken place at 59–62 Ma. The north-west Mull lava pile, which is part of the MPLF (Fig. 2) is exposed as a relatively thin (~250 m) succession of compound flow lobes, inflated pahoehoe (Kent et al., 1998) and tabular sheet flows with some minor intrusions (Kerr et al., 1999; Pugsley, 2021). Samples for this study were collected from the area from Ulva Ferry around the coastline to north of Calgary Bay (Fig. 2). Virtual outcrop models were constructed using drone-based photogrammetry along the coastal section from south Beinn Reudle to east of Caliach Point to aid with stratigraphical correlation (Fig. 2). The lava field has been subjected to significant late, mostly normal faulting, dividing it into a series of fault blocks. In addition to the virtual outcrop the area was mapped from the ground with numerous logs of the lava field providing additional data with which to develop a stratigraphical model. The virtual outcrop and field data allow broad stratigraphical correlations to be made across the area. Distinct NW-SE lineaments are visible cutting the entire region and the lava field morphology is consistent with an origin by effusion from a series of fissures corresponding with the lineaments. The full details of the stratigraphy of the lava pile will be published elsewhere. Petrographically, the NWM lower lavas are typical of the olivine-phyric lavas of BPIP plateau type. The NWM upper lavas are aphyric and fine-grained and comprise flow-aligned plagioclase with interstitial augite and rare olivine.

3. Analytical methods

Whole-rock samples from NW Mull (NWM) were analyzed using XRF (ThermoARL Advant'XP+) and ICP-MS (HP 4500+) at the Peter Hooper GeoAnalytical Laboratory at Washington State University (WSU). Technical notes and principles of these methods have been described by Johnson et al. (1999) and Knaack et al. (1994). Tabulated details of analytical precision, accuracy and duplicates analyses performed during this study are given in supplementary materials. For trace elements by ICP-MS precision is typically 0.53–1.93% relative standard deviation, and accuracy better than 7% relative percentage difference based on duplicate analyses over five years. International reference samples AGV2, BCR2 and GSP-2 were run as unknowns during the period of this study and data are given in the supplementary materials. Samples collected from Ulva, including the low Y mugearite, were originally reported in Hole et al. (2015) with XRF major and trace element data from the Open University UK. We have re-crushed and re-analyzed these samples at WSU. Excepting of minor differences in SiO_2 (<0.8% absolute) data are in good agreement between the two laboratories.

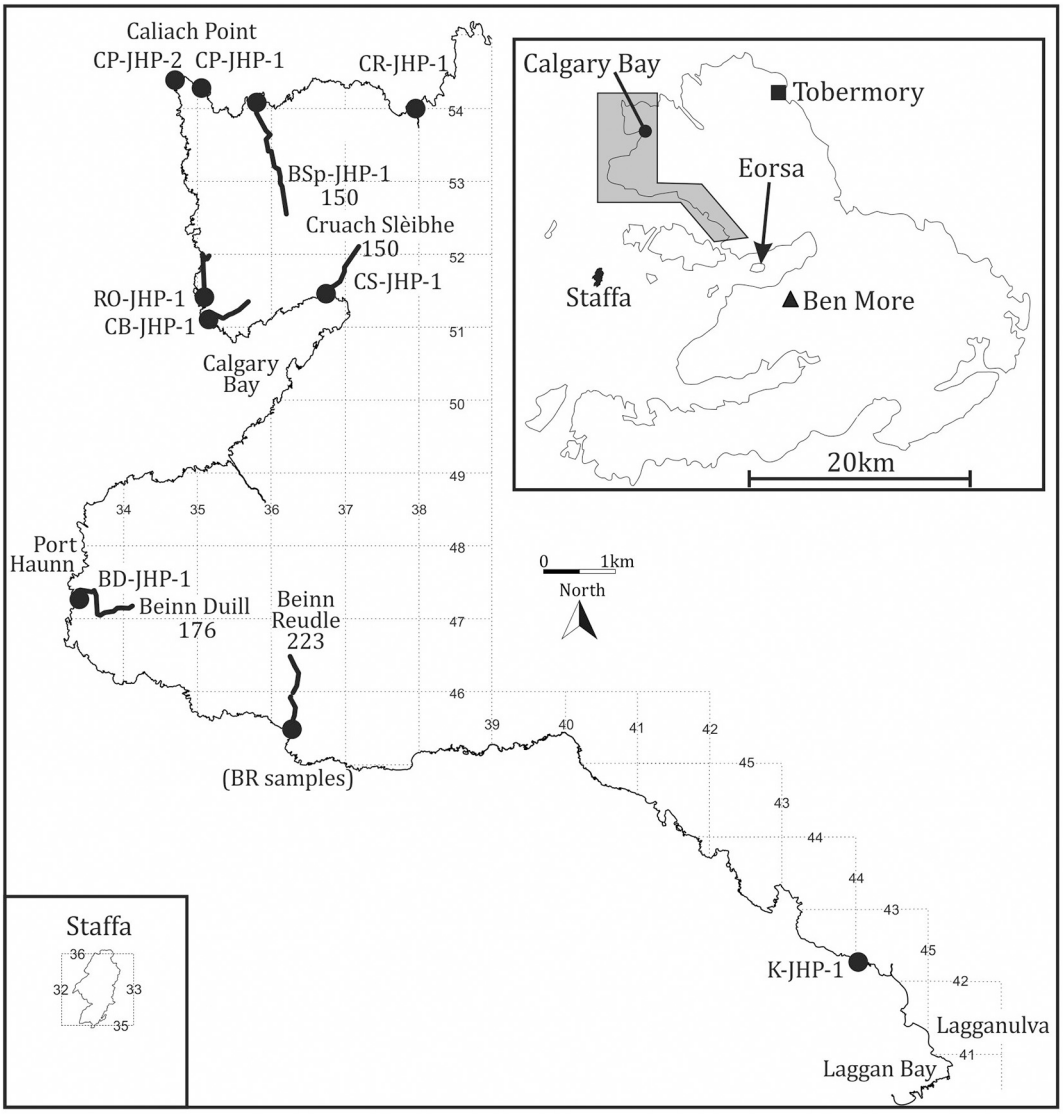

Fig. 2. Maps of Mull showing samples localities mentioned in the text. Detailed locations and grid references for each of the analyzed samples are given in the supplementary material.

4. Geochemistry of the lavas

According to the total alkalis-silica classification of Le Maitre et al. (2002) samples analyzed in this study are basalts or hawaiites. Lavas are silica-saturated (*Hy*-normative) to mildly silica-undersaturated (*Ne*-normative) and occupy a position in the expanded CIPW normative tetrahedron (Fig. 3) of Thompson (1982) which is typical of Hebridean plateau-type lavas related to a ~ 0.90 ± 0.15 GPa cotectic (e.g., Hole et al., 2015; Thompson, 1982).

Four samples of low Y mugearite analyzed in the current study have near-identical chemical compositions and are likely to be the same lava flow (supplementary material). These were collected from Lagganulva, Eorsa and Ulva Ferry (Fig. 2). Using the scheme of Le Maitre et al. (2002) these are more strictly classified as a hawaiite. However, occurrences of similar low Y intermediate lavas along the same section of coastline as K-JHP-1.1 were classified as 'low-Y mugearites' by Thompson (1982), Kerr et al. (1995, 1999, samples P7 and UV2e) and Beckinsale et al. (1978; samples R18, R154 and M169) and these samples straddle the hawaiite-mugearite divide. For consistency with previously published descriptions we retain the term 'low-Y mugearite' in this study.

Covariations between MgO and other major elements are shown in Fig. 4 and are compared with data for lavas from Beinn Reudle (Fig. 2). Geochemical data for Beinn Reudle were reported by Kerr et al. (1999) and our field investigations identify the Beinn Reudle and Beinn Duill (Fig. 2) as stratigraphical correlatives. We therefore augment our new data set with published data from Beinn Reudle. Also included in Fig. 4 are data for lavas of the Staffa Lava Formation (SLF) and intrusions of the Loch Scriddain Sill Complex (LSSC) both of which are part of the Mull magmatic system. The SLF immediately underlies the MPLF and it is well established that both SLF and LSSC magmas crystallized under near-surface conditions (Hole et al., 2015; Kerr et al., 1999; Preston et al., 1998; Thompson et al., 1986) and these data are used to provide a comparison with the NWM data.

Data for FeO_T and MgO reveal two distinct lineages of lavas from NW Mull (Fig. 4d), a high FeO_T group (FeO_T > 13 wt% and MgO 4–9 wt%) and a lower FeO_T group (10–13 wt%) the latter of which is generally more mafic (MgO 6–16 wt%). Whilst there is some scatter in the covariation of height (metres above mean sea level) versus FeO_T (Fig. 4h), which can be attributed to local normal faulting, the high FeO_T lavas are mostly restricted to the upper parts of the stratigraphy of the lava pile (Fig. 4h); at heights <120 m most samples are low FeO_T. Henceforward these will be referred to as NWM lower (<120 m; low FeO_T) and NWM upper (>120 m; high FeO_T) lavas respectively. Near the base of the exposed lava pile is a brown-red matrix-supported volcanic

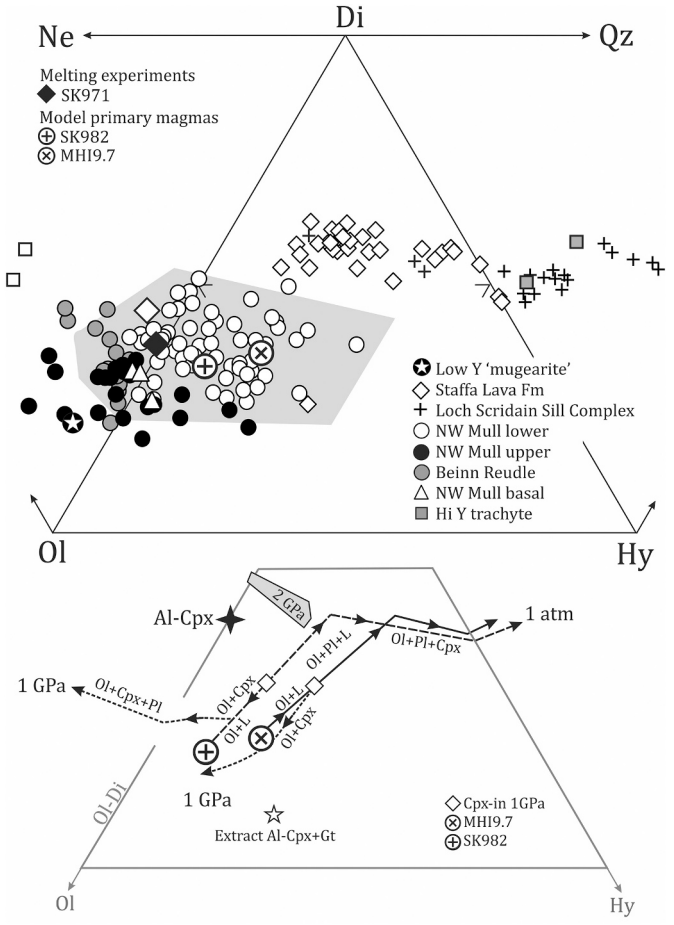

Fig. 3. CIPW normative tetrahedron projected from or towards plagioclase, plotted following the method of Thompson (1982) for a) Mull lavas and sills. Data sources; NW Mull upper and lower, this study; Ben More and other trachytes Kerr et al. (1999); Loch Scridain Sill Complex, Preston et al. (1998); Staffa Lava formation, Thompson et al. (1986); Kerr (1998). The grey shaded area encompasses the compositions of Mull Plateau Lava Formation and Skye Lava Group (Williamson and Bell, 1994; Williamson and Bell, 2012). Crosses in circles are two model primary magma compositions from Hole and Millett (2016); orthogonal cross, SK982; diagonal cross, MHI9.7. The normative compositions of SK971 which was used in the melting experiments of Thompson (1974) is shown for reference. b) map showing the general fractionation trajectories from model primary magmas representing small (SK982; F-AFM = 0.16) and large (MHI9.7; F-AFM = 0.24) melt fractions at 1 atm and 1 GPa. Liquid lines of descent (LLD) were generated using Petrolog3 (Danyushevsky and Plechov, 2011) using the QFM buffer of Kress and Carmichael (1988), the (pressure sensitive) olivine model of Herzberg and O'Hara (2002), plagioclase and clinopyroxene melt liquidus associations of Danyushevsky (2001). Four-point star is Al-Cpx (14.5 wt% Al_2O_3 6.5% CaTs) from Thompson (1974) and the field labelled 2 GPa is for Al-Cpx (14.0–15.5 wt% Al_2O_3 ~ 6% CaTs) in equilibrium with garnet from Liu and Presnall (2000). The extract (white star) is for 59% Al-Cpx + 41%Gt and is discussed in the text.

clast-dominated conglomerate approximately 5 m thick. Lavas immediately above and below the conglomerate, some of which may be invasive, are high FeO_T, (Fig. 4h) and these will be referred to as NWM basal lavas. High FeO_T lavas are not a feature of the LSSC of SLF, both of which exhibit FeO_T < 12 wt% at ~5 wt% MgO (Fig. 4d).

NWM Lower and upper lavas are also distinguished in terms of covariations between SiO_2 and MgO (Fig. 4a), with the upper lavas exhibiting a negative covariation offset to lower MgO. Similar distinctions between upper and lower lavas are evident for TiO_2 with the upper lavas having TiO_2 in the range 1.9–3.3 wt%, compared to 1.1–1.9 wt% TiO_2 for the lower lavas. Covariation between MgO and Al_2O_3 is negative and near linear over the range 16–7.5 wt% MgO (Fig. 4c), for both upper and lower lavas, and Al_2O_3 reaches a plateau value of ~17.5 wt% at ~7.5 wt% MgO. By contrast SLF and LSSC samples with <8 wt% MgO have lower Al_2O_3 (14.0–15.8) than the upper and lower lavas. Covariations between MgO and CaO show that NWM lavas have consistently lower CaO for a given MgO content compared to lavas of the SLF and LSSC. The low Y mugearites are the most evolved samples in the data set (MgO = 3.0 wt%; Mg# = 31) and in Fig. 4 fall at the end of the data array for the upper lavas.

Zr, Nb and La behave incompatibly during crystallization (Fig. 5a-c) with well-defined curvilinear covariations with MgO; the NWM upper and lower lavas, SLF and LSSC samples all fall on approximately the same trends for these elements. The behaviour of Sr, Yb and Sc is more complex. Some of the scatter in the MgO-Sr diagram is probably the result of zeolite facies alteration, particularly in amygdaloidal compound lava flows. However, Sr behaves broadly incompatibly in NWM lavas with <~8 wt% MgO (Fig. 5d). LSSC and SLF samples have considerably higher Sc abundances (30–50 ppm) for a given wt% MgO compared to NWM upper (Sc =5–26 ppm) and lower (Sc = 30–36 ppm) lavas (Fig. 5f). MgO-Yb covariations exhibit a bifurcation at ~7 wt% MgO (Fig. 5e) as originally described by Kerr and Thompson (1995) such that in some of the lower lavas the bulk partition coefficient (D) for Yb ≥ 1. Again the 'low Y mugearite' is at the extreme end of the trends for the upper lavas. By contrast SLF lavas exhibit enrichment in Yb consistent with DYb < <1.

Chondrite-normalized REE patterns for NWM lavas from the Cruach Sleibhe section (Fig. 2) are shown in Fig. 6. This stratigraphical section has been chosen for scrutiny because it represents the most complete stratigraphical section from sea level up to ~120 m. All samples are light rare earth element (LREE) enriched, with chondrite-normalized La/Yb ($[La/Yb]_N$) in the range 1.6–12.2 (Fig. 6). The majority of lavas have $[La/Sm]_N < 1.0$ but $[Sm/Yb]_N > 1.0$ producing a curved REE pattern that is characteristic of Hebridean lavas and is best explained by variable extents of melting of LREE-depleted mantle peridotite in the garnet-spinel transition of the upper mantle (e.g. Hole et al., 2015; Kerr et al., 1999; Thompson, 1982). However, the basal lavas and some lower lavas have $[La/Sm]_N$ up to 2.1 (Fig. 6c). At Cruach Sleibhe, NWM upper lavas exhibit increasing abundances of LREE but decreasing abundances of HREE with decreasing Mg#, the low Y mugearite being an extreme example of LREE enrichment with $[La/Yb]_N$ ~ 32. It is worthy of note that samples BD-JHP-1.14 (Beinn Duill) and BR18 (Beinn Reudle; Kerr et al., 1999) are indistinguishable from sample CS-JHP-1.12 in terms of REE abundances and are thus considered to be stratigraphical equivalents (supplementary materials).

Primitive mantle-normalized (Sun and McDonough, 1988) multi-element plots (Fig. 7) clearly distinguish between the NWM basal, lower and upper lavas. NWM basal and lower lavas exhibit strong negative anomalies for Th, U, Nb and Ta compared to adjacent elements with La/Ta in the range of 37.5–58.0 and Th/Ta 1.7–2.4. By contrast, the NWM upper lavas do not exhibit such an anomaly and have La/Ta =16.5–21.0 and Th/Ta in the range of 0.95–1.8 producing a smooth convex-upwards profile in Fig. 7a.

5. Discussion

5.1. Major and trace element constraints on order of crystallization

Thompson (1982) noted that in terms of normative compositions the ~1GPa liquid-line-of-descent (LLD) of typical Hebridean *hy*-normative primitive lavas crosses the Ol-Di join and progresses towards *ne*-normative compositions with decreasing temperature. In contrast, at near-surface pressure, the same primitive lava composition follows a LLD that ultimately crosses the Di-Hy join and progresses towards Qz-normative compositions (Fig. 3). Fig. 3b shows Petrolog3 simulations of crystallization from model primary magmas to Skye lava SK982 and Islay lava MHI9.7 (Hole et al., 2015; Hole and Millett, 2016) at 1 atm

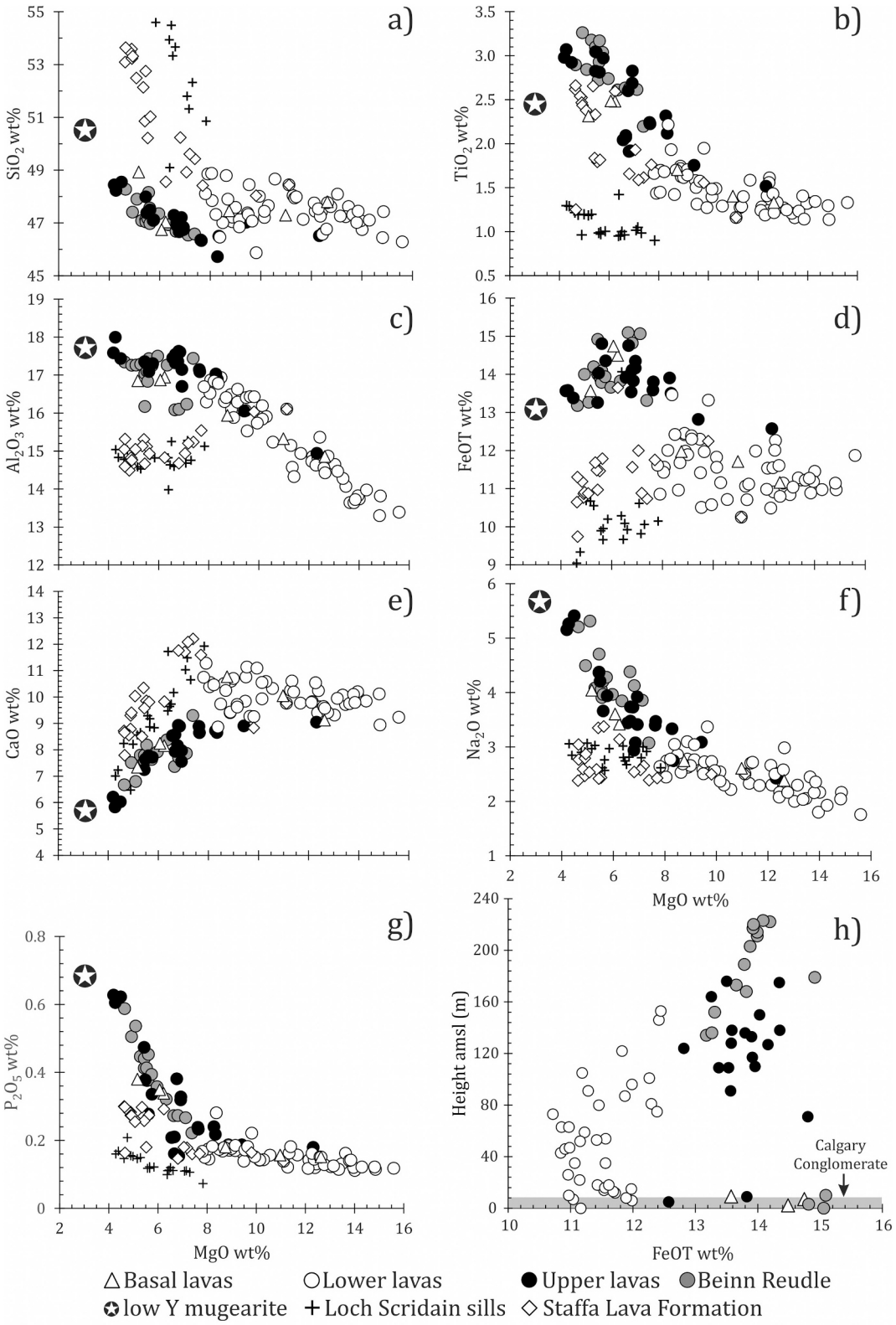

Fig. 4. Major element variations in north Mull lavas from this study and Ben Reudle from Kerr et al. (1999). Data for the Loch Scridain Sill Complex (LSSC) is from Preston et al., 1998 and Staffa Lava Formation (SLF) is from Thompson et al. (1986) and Kerr (1998). The star in the circle encompasses the four low Y mugearites analyzed in this study.

and 1 GPa. These model primary magmas were chosen because they represent typical examples of Hebridean model primary magmas with melt fractions of 0.16 (SK982) and 0.24 (MHI9.7). Petrolog3 faithfully reproduces the opposing down-temperature trends described by Thompson (1982) which result from the change in order of crystallization from Ol → Plag→Cpx at 1 atm to Ol → Cpx → Plag at ~1 GPa (Fig. 1a). The position occupied by the NWM lavas in Fig. 3 is broadly consistent with crystallization ~1 GPa, and magmas of the SLF and LSSC

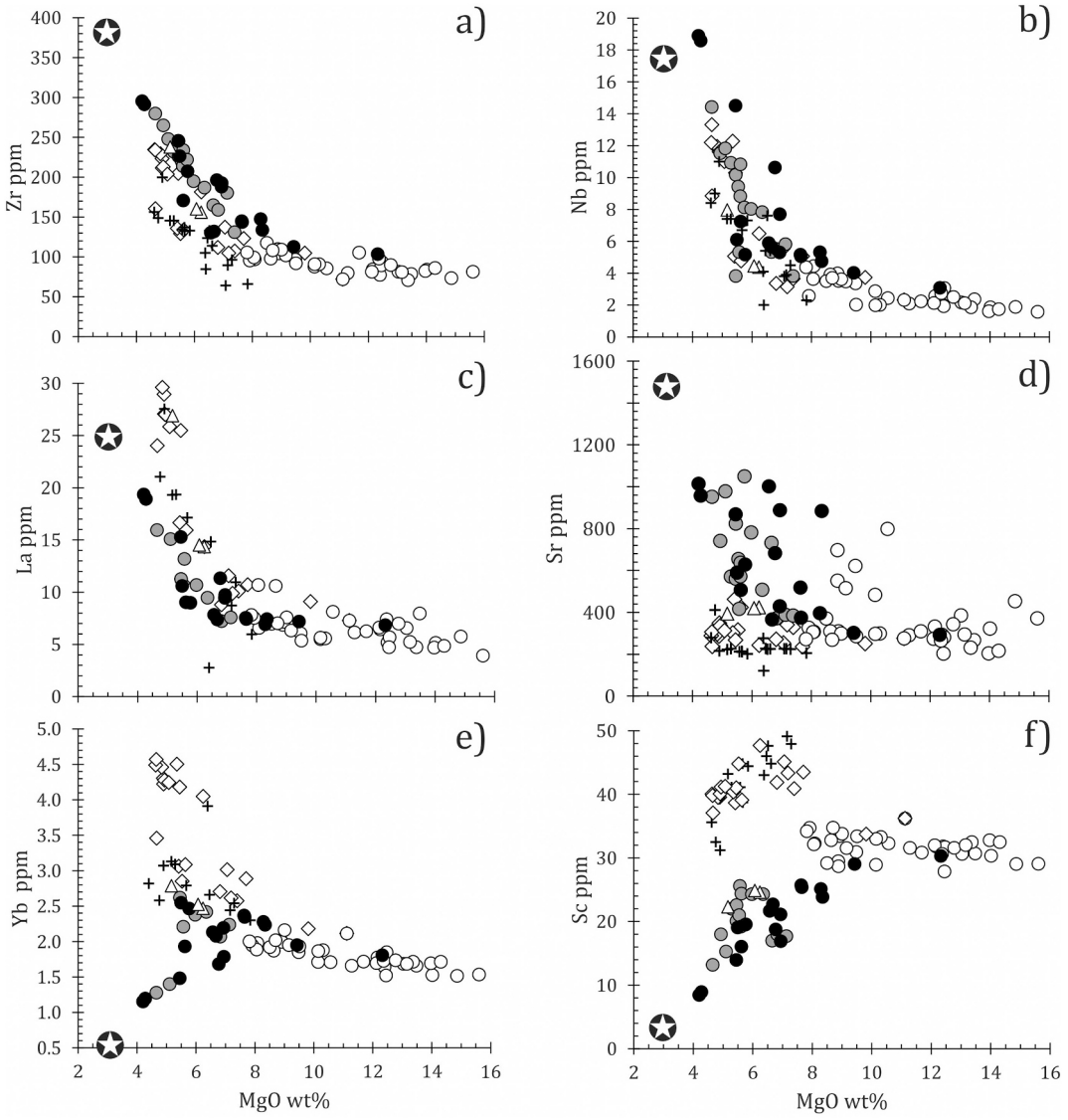

Fig. 5. Selected trace elements versus MgO wt% in north Mull lavas symbols and data sources as in Fig. 4.

follow a low pressure near 1 atm trend.

Normative variations are necessarily expressed in the contrasting behaviour of SiO_2, CaO and Al_2O_3 (Fig. 4c) between NWM lavas and SLF and LSSC lavas. The *ne*-normative character of the NWM lavas is reflected in lower SiO_2 for a given MgO content compared to the silica-saturated, *hy*-normative nature of the SLF and LSSC lavas. Similarly, early clinopyroxene crystallization at >1 GPa results in NWM lavas with lower CaO for a given MgO content compared to lavas that crystallize at near-surface pressures (Fig. 4e). Additionally, Al_2O_3 is consistently higher ($Al_2O_3 \sim 17.5$ wt%) in NWM lavas with <8 wt% MgO than SLF and LSSC lavas with the same range of MgO contents, which contain 14.0–15.6 Al_2O_3 wt%. This suggests that plagioclase joined the crystallizing assemblage at lower MgO content in the NWM lavas compared to lavas of the SLF and LSSC.

The incompatibility of Sr in NWM upper and lower lavas compared to SLF lavas with similar MgO contents also suggests suppression of plagioclase crystallization in the NWM lavas (Fig. 5d). Sc is variably compatible with clinopyroxene ($k_DSc^{Cpx/L} = 0.84–1.51$; Le Roux et al., 2015) but incompatible with respect to olivine and plagioclase ($k_DSc^{Ol/L} < 0.01$; $k_DSc^{Pl/L} < 0.1$). Consequently, SLF and LSSC magmas, which likely crystallized olivine and plagioclase at low pressures, have higher Sc abundances for a given MgO content than the NWM lavas because the latter are likely to have undergone early clinopyroxene fractionation at pressure ≥ 1GPa. However, since Sc is strongly compatible with garnet ($k_DSc^{Gt/L} \sim 6$; Le Roux et al., 2015), garnet crystallization might have contributed to the low Sc abundances in the most evolved NWM upper lavas. Additionally, the compatibility of the HREE but incompatibility of LREE for the NWM upper lavas (Figs. 5e and 6a) requires crystallization of a phase with DHREE> > DLREE for which garnet is also the most likely candidate. The incompatibility of Zr in NWM lavas (Fig. 5a) precludes the explanation of Thompson et al. (1980) that zircon crystallization was responsible for extreme LREE-enrichment in benmoreites from other locations in the BPIP.

Overall, geochemical variations and normative characteristics require an order of crystallization of Ol → Cpx → Pl for the NWM lavas and Ol → Pl → Cpx for the SLF and LSSC magmas which is consistent with crystallization at ≥1 GPa for NWM lavas and ~ 1 atm for the SLF and LSSC magmas. However, because the order of crystallization of the main liquidus phases does not change significantly between 1.0 and 1.8 GPa (the pressure at which garnet becomes a stable phase) normative characteristics only provide an estimate of the minimum pressure of crystallization of the NWM lavas.

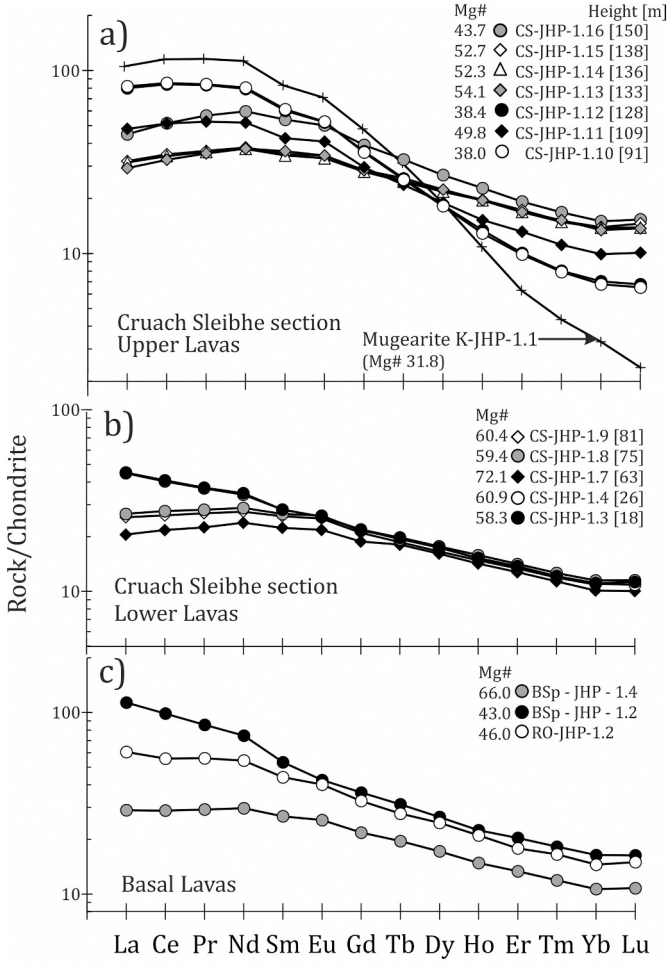

Fig. 6. Chondrite-normalized REE patterns for a) NWM upper lavas; b) NWM lower lavas and c) NWM basal lavas. a) and b) are from the Cruach Sleibhe section, North Mull (Fig. 1). K-JHP-1.1 is the mugearite from Ulva Ferry. Mg# are given in the legend. Note that BD-JHP-1.14 (Beinn Duill) and BR18 (Beinn Reudle; Kerr et al., 1999) are indistinguishable from CS-JHP-1.12 and are thus considered to be stratigraphical equivalents. See supplementary data for details.

5.2. Crustal contamination

It is well-established that many BPIP magmas underwent interaction with continental crust of varying ages and compositions (e.g., Hole et al., 2015; Kerr et al., 1995; Thompson et al., 1986). Processes such as assimilation with fractional crystallization (AFC; DePaolo, 1981) and assimilation with turbulent ascent (ATA; Kerr et al., 1995) will mask the geochemical trends generated by fractional crystallization alone and in this study, we need to be as certain as possible which lavas are related to one another by simple fractional crystallization alone.

Inter-element ratios of Th, Ta and La are good indicators of crustal contamination in Hebridean lavas and exhibit strong correlations with isotopic compositions (e.g., Dickin et al., 1987; Hole et al., 2015; Kerr et al., 1995; Thompson et al., 1982; Thompson et al., 1986). Consequently, it is possible to assess the role of crustal contamination using trace elements alone. Hole et al. (2015) and Thompson et al. (1982) showed that isotopically uncontaminated Hebridean lavas are characterized by La/Ta < 30 and Th/Ta <2, εNd up to ~ + 8 and $^{206}Pb/^{204}Pb$ ~ 17.5. By Contrast, lavas containing unradiogenic Nd (εNd < 0) and unradiogenic Pb ($^{206}Pb/^{204}Pb$ ~ 16.0) were contaminated with Lewisian granulite resulting in La/Ta >50 and Th/Ta < 2 (Fig. 8). On primitive mantle-normalized multi-element diagrams (Fig. 7), contamination with Lewisian granulite results in a marked trough at elements Th, U, Nb and

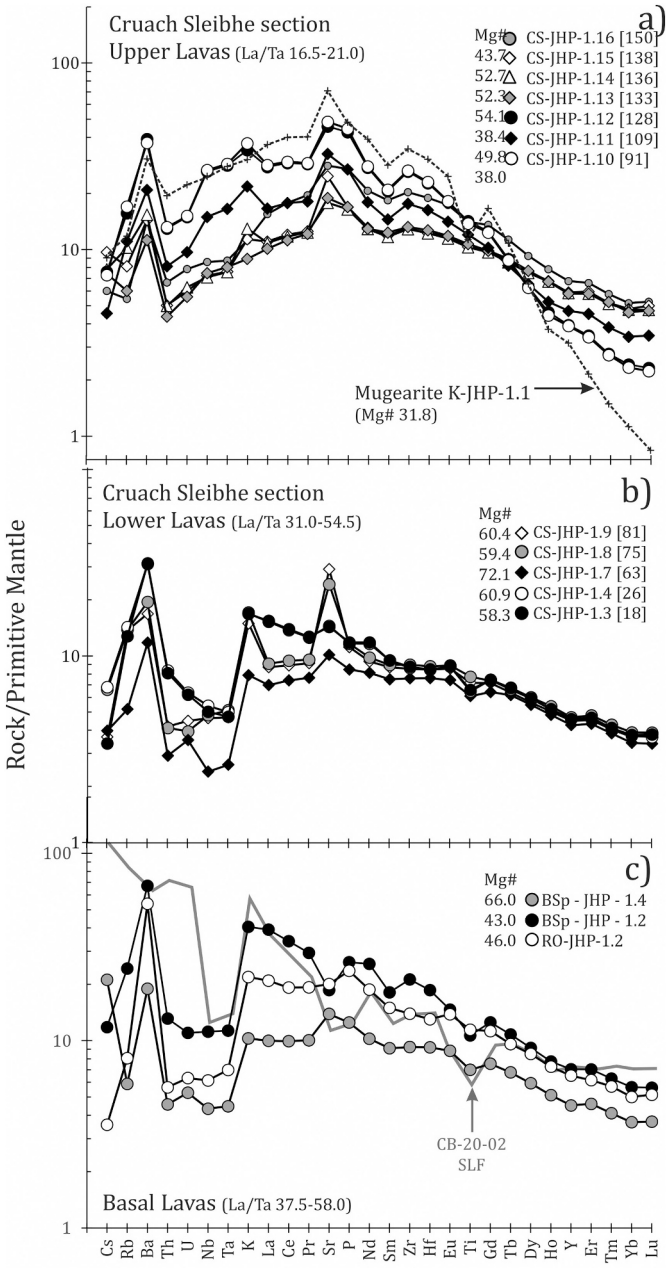

Fig. 7. Primitive mantle-normalized (Sun and McDonough, 1988) multi-element plots for the same samples as shown in Fig. 6.

Ta compared to adjacent elements giving high La/Ta but low Th/Ta (Fig. 8). Lavas contaminated with Moine or other metasedimentary rocks again exhibit εNd < 0, but contain radiogenic Pb ($^{206}Pb/^{204}Pb$ up to 19.0) and have Th/Ta up to ~10 and La/Ta up to ~50 (e.g., Staffa lavas; Jolley et al., in press) resulting in a marked trough only for Nb and Ta and not for U and Th on primitive mantle-normalized diagrams (e.g. SLF; Fig. 7c).

Figs. 7 and 8 show that the NWM basal and lower lavas must have undergone significant crustal contamination with Lewisian-type contaminants or with a combination of Lewisian and Moine-type contaminants to produce their elevated La/Ta and Th/Ta. Conversely, the upper lavas are more evolved than the lower lavas and have La/Ta <30 and Th/Ta <2.0 consistent with negligible amounts of crustal contamination. It is striking that the NWM basal and upper lavas have a similar range of MgO (5–7 wt%) but very different La/Ta (basal lavas >50; upper lavas <30) implying significantly more contamination of the basal

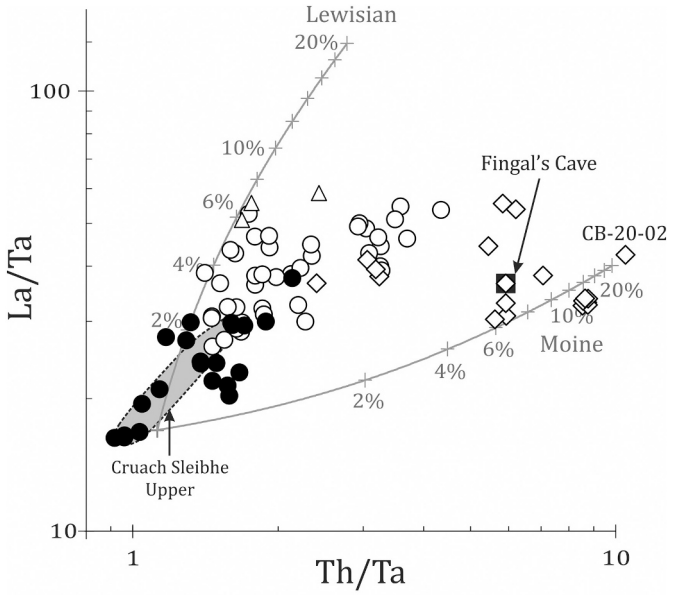

Fig. 8. La/Ta versus Th/Ta for North Mull lavas. Grey lines and crosses represent mixing trajectories between a mantle-derived magma and Lewisian granulite and Moine pelite as labelled. After Hole et al. (2015). The range for Cruach Sleibhe upper lavas is indicated. Symbols and data sources as for Fig. 4.

than upper lavas over a similar range of MgO. The relationship between FeO_T and stratigraphical position (Fig. 4f) therefore requires that the basal high FeO_T lavas have a different petrogenetic history from the upper lavas with similar FeO_T.

Overall, there is no trace element evidence to suggest that the NWM upper lavas have undergone any significant interaction with continental crust of any type and the trace element characteristics illustrated in Figs. 7 and 8 are near-identical to Mull and Skye lavas identified by Thompson (1982) as being 'pristine' melts of mantle peridotite. Consequently, and given the close stratigraphical relationship between the upper lavas, we argue that the NWM upper lavas represent the products of a single LLD of a mantle-derived magma that underwent no significant crustal contamination. The remainder of this paper will focus on the petrogenesis of the least contaminated upper lavas.

5.3. Numerical pressure estimates from the An-Di-En molecular projection

Herzberg (2004) provides a petrological method estimating the pressure of crystallization that is based on a parameterization of experimental data in the form of a projection from or towards olivine onto the plane diopside-anorthite-enstatite (Di-An-En), calibrated to 1 GPa (Fig. 9). Lavas must be saturated with Ol + Cpx + Pl for pressure estimates to be made and we use a data set comprising Mull samples with <7 wt% MgO. The effect of increasing pressure is to increase the Al_2O_3 content of liquids on the olivine gabbro cotectic, and this is manifested in higher plagioclase contents when viewed in projection. Herzberg (2004) showed that loci of liquid compositions on the [L + Ol + Plag+Aug] cotectics shown in Fig. 9 are parameterized from the experimental data with the following equation;

$$An = 52.95 + 10.08P + 1.58P^2 - 0.4645En \quad (1)$$

where An and En are molecular projection coordinates. In Fig. 9 whether LLDs project to the left or right along cotectics is dependent on the Si-saturation of the primary magma; in general, Si-undersaturated compositions move to the left and Si-saturated compositions to the right (Herzberg, 2004).

Residual liquids from the melting experiments on sample I260 conducted by Whitaker et al. (2007) at ~1 GPa and 1 atm are shown in Fig. 9a. Note that the Whitaker et al. (2007) experiments post-date the Herzberg (2004) parameterizations and can therefore be used to independently assess the accuracy of the method. The Whitaker et al. (2007) experimental results agree well with the parameterizations of Eq. (1) at both 1 atm and ~ 1 GPa, as do the residual liquids from the experiments of Thompson (1974) on Skye lavas 66,018 (alkali basalt; 11.08 wt% MgO) and SK971 (transitional basalt; 7.69 wt% MgO) at 0.8–1.0 GPa (Fig. 9a). Additionally, Petrolog3 (Danyushevsky and Plechov, 2011) simulations of crystallization at 1 atm and 1 GPa for the two model primary magmas shown in Fig. 3b show good agreement to the cotectics in Fig. 9a. Although the original parameterizations of Herzberg (2004) were only calibrated to 1 GPa, we have calculated the position of cotectics in Fig. 9 up to 1.4 GPa using Eq. (1). Residual liquids from the experiments of Thompson (1974) conducted on Skye lavas at ~1.2 GPa fall close to the calculated 1.2 GPa isobar. Petrolog3 simulations at 1.4 GPa plot closer to an estimated 1.6 GPa cotectic in Fig. 9a and this mismatch suggests the application of Eq. (1) becomes doubtful above ~1.2 GPa. Also shown in Fig. 9a are data for the 2 GPa crystallization experiments of Liu and Presnall (2000). Cotectic compositions comprising garnet + diopside + enstatite ± sapphirine (Gt + Di + En ± Sa) fall close to the 1.2 GPa isobar in the region for silica-saturated systems. Indeed, all the experimental liquids produced by Liu and Presnall (2000) are Qz-normative, Si-oversaturated compositions and thus may not be the best analogies for BPIP primary magmas. Nevertheless, garnet-bearing cotectic compositions do indeed fall towards the *An* apex of Fig. 9 indicating crystallization at >1.2GPa.

Data for NWM upper lavas (including Beinn Reudle) containing <7 wt% MgO fall above the 1GPa cotectic and cluster around our calculated cotectics at 1.2–1.4 GPa (Fig. 9b) which is in sharp contrast to data for SLF and LSSC which are both related to low pressure cotectics at <0.4 GPa (Hole et al., 2015; Thompson, 1982). Basal lavas (~4.5 wt% MgO) along with K-JHP-1.1 (3.0 wt% MgO) plot at a pressure > 1GPa. NWM lower lavas all have MgO in the range 8.5–14.8 wt% and cannot therefore be included in Fig. 9. However, Hole (2018) showed that trace elements in olivine from Beinn Reudle sample BR6 (13.7 wt% MgO) are consistent with crystallization at ~1.6 GPa and we are therefore confident that NWM upper lavas must have crystallized at ≥1.2 GPa.

Experimental liquids in equilibrium with (Gt + Di + En ± Sa) at 2 GPa fall along an extension of the array for north Mull lavas to higher *En* contents. All evidence from Fig. 9 points to crystallization of the NWM upper lavas and low Y mugearite at a pressure > 1.2 GPa. We now turn to an examination of the potential role of garnet in the generation of the upper lavas.

5.4. Garnet and Al-Cpx fractionation - the system CMAS

To assess the relative roles of garnet and clinopyroxene during crystallization we utilize the projection from or towards olivine onto the plane CS-MS-A (Fig. 10) of O'Hara (1968) which allows the projection of garnet and Al-Cpx from experimental data relative to measured lava compositions. At ~1 atm the crystallization sequence is L + Ol and then L + Ol + Pl which will result in an LLD that projects from a primary magma composition (Fig. 10) towards the MS-CaTs join (O'Hara, 1968). Once the cotectic L + Ol + Pl + Cpx is reached, the LLD progresses along the MS-CaTs join. Whether the LLD progresses towards CaTs or MS is dependent on the primary magma composition, Si-undersaturated compositions moving towards CaTs and Si-saturated compositions towards MS.

At ~1 GPa the crystallization sequence is L + Ol → L + Ol + Al-Cpx → L + Ol + Al-Cpx + Pl. The net effect is an LLD that projects along the MS-CaTs join for the final cotectic assemblage (Fig. 10). Again, the position of the starting composition controls whether the LLD projects towards MS (Si-oversaturated) or CaTs (Si-undersaturated), as is the case for the CIPW NORM (Fig. 3). For BPIP plateau-type magmas crystallizating at >1GPa the LLD projects towards CaTs, following an Si-undersaturated trend. The position along the MS-CaTs join towards

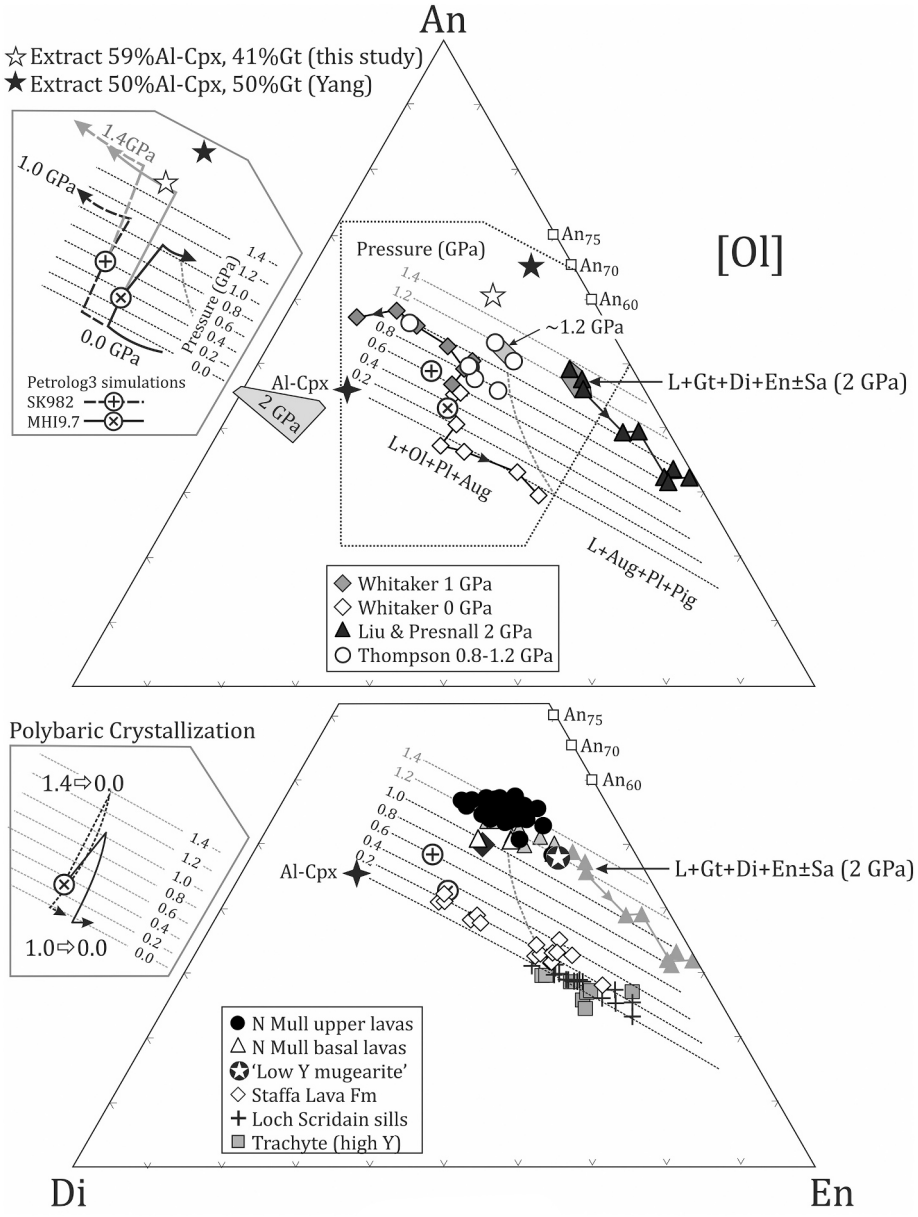

Fig. 9. Molecular projections to or from olivine onto the plane Di-An-En (diopside-anorthite-enstatite). Isobars were calculated according to the scheme of Herzberg (2004). The grey pecked curve is the thermal divide between olivine gabbro and norite. a) residual liquids from the crystallization of olivine+plagioclase+augite at 0.00 and 0.93 GPa from the melting experiments of Whitaker et al. (2007). Black triangles are residual liquids from the 2 GPa melting experiments of Liu and Presnall (2000), liquids in equilibrium with garnet+Al-Cpx + enstatite±sapphirine are indicated in the grey shaded area. Inset; Petrolog3 simulations from model primary magmas MHI9.7 and SK982 (Hole and Millett, 2016) at 0.0, 1.0 and 1.4 GPa. Petrolog3 melt-liquidus models used were; olivine, Herzberg and O'Hara (2002); plagioclase and clinopyroxene, Danyushevsky (2001). QFM-1 (Kress and Carmichael, 1988). Four-point black star is Al-Cpx (2 GPa) from Thompson (1974) and the shaded box labelled "2 GPa" is for Al-Cpx in equilibrium with garnet (Liu and Presnall, 2000). b) The same projection for NWM upper and basal lavas, LSSC, SLF and trachytes from Ben More (Kerr et al., 1999). Extracts are the estimated proportions of Al-Cpx and Gt contributing to the fractionating assemblage for this study (Table 1) and Yang et al. (2023). Inset, lower-left; two-step polybaric crystallization models calculated using Petrolog3 from model primary magma MHI9.7. Steps are; 1.4 GPa, F = 1.0–0.7 then 0.0 GPa; 1.0 GPa, F = 1.0–0.7 then 0.0 GPa. Projection code (mole %); An = Al_2O_3 + TiO_2; Di = CaO + Na_2O + $3K_2O$ – Al_2O_3; En = SiO_2_$0.5Al_2O_3$_0.5FeO − 0.5MnO − 0.5MgO (Herzberg, 2004).

CaTs is largely controlled by total alkalis (Na_2O + K_2O) in this projection, such that with increasing total alkalis lavas project farther towards CaTs. Because plagioclase is the main Na_2O-bearing phase in basaltic systems, suppression of plagioclase crystallization at high pressures results in increasing Na_2O contents and thus an LLD that projects towards CaTs. At > ~ 1.8 GPa garnet will replace plagioclase as the main aluminous phase in the system. Data for garnet and Al-Cpx from 2 and 3 GPa melting experiments (Liu and Presnall, 2000; Thompson, 1974; Yang et al., 2023) are shown in Fig. 10. Initial crystallization of Ol + Al-Cpx, before garnet joins the crystallizing assemblage, from any reasonable starting composition will drive the LLD towards the MS-CaTs join. Data for the NWM upper lavas and the experimental cotectic glasses of Liu and Presnall (2000) all project close to the MS-CaTs join, but data for the Mull lavas project towards CaTs and the experimental glasses towards MS. This is a predictable consequence of differences in the Si-saturation of the starting compositions (Fig. 10) the Mull lavas being part of a silica-undersaturated LLD.

Projection along the CaTs-MS join in either direction requires that the bulk composition of the cotectic extract, comprising Al-Cpx + Gt at >1.8 GPa, also projects close to the CaTs-MS join. A simple least-squares

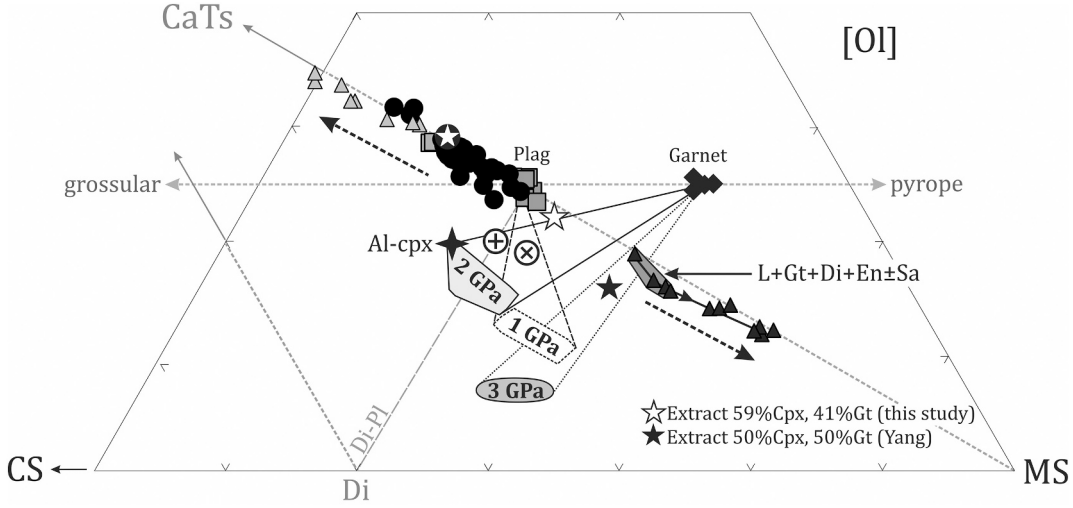

Fig. 10. Molecular projections from or towards olivine on to the plane CS-MS-A. CaTs is calcium Tschermakite ([CaAl][AlSi]O_6). Shaded boxes labelled with pressure are Al-Cpx compositions from Whitaker et al. (2007), Liu and Presnall (2000) and Yang et al. (2023). Other symbols as for Fig. 10. Pecked arrows indicate down-temperature crystallization. Projection code (mole %); CS = CaO+(2Na_2O + K_2O) – 3.333P_2O_5; MS = 2SiO2 + TiO2 – (FeO + MnO + MgO) – 2CaO – 8(Na_2O + K_2O) + 6.666P_2O_5; A = TiO_2 + Al_2O_3 + Na_2O + K_2O (O'Hara, 1968).

mixing model (Table 1) for parent lava BD-JHP-1.14 (8.34 MgO) to daughter lava BD-JHP-1.16 (5.45 wt% MgO) crystallizing 2.0 GPa Al-Cpx and garnet from Thompson (1974) along with plagioclase An_{70} and olivine Fo_{80}, yields 59% Cpx and 41% Gt as the crystallizing assemblage with negligible An_{70} and Fo_{80} ($\sum^2$ residuals = 0.52). This extract falls close to the MS-CaTs join (Fig. 10) and thus would be capable of producing the observed LLD. However, this is not a unique solution as a plagioclase-dominated assemblage would also produce the observed LLD.

In summary, the data for NW Mull upper lavas containing <7 wt% MgO presented in Figs. 9 and 10, indicate cotectic crystallization at >1.6 GPa. Additionally, at ~1.8 GPa an extract of approximately 59% Al-Cpx and 41% garnet would be capable of producing the observed major element variations in the NW Mull upper lavas. However, because the CMAS projection in Fig. 11 cannot distinguish between LLDs resulting from crystallization of Al-Cpx + Pl and Al-Cpx + Gt, we must turn to trace elements which are more sensitive to Al-Cpx or Gt fractionation.

5.5. *Trace element evidence for fractional crystallization of garnet*

Upper lavas exhibit increasing LREE-enrichment with decreasing MgO with, for example, $[Nd/Yb]_N$ increasing from ~2 to 32 over the range 7–3 wt% MgO (Fig. 11a). Consideration of chondrite-normalized REE patterns (Fig. 6) also shows that increasing $[Nd/Yb]_N$ is a function of both increasing LREE and decreasing HREE abundances with decreasing MgO (see also Fig. 5e). Furthermore, REE profiles (Fig. 6c) rotate around Dy which requires a bulk partition coefficient for Dy~1 in the crystallizing assemblage.

Partition coefficients for garnet and basaltic liquids are well-known and garnet fractionates the LREE relative to HREE. It is accepted that $k_DLa^{Gt/L} < 0.01$ and $k_DLu^{Gt/L} \sim 10$ (e.g., Hole et al., 2023; McKenzie and O'Nions, 1995; Pertermann et al., 2004) and the change in REE behaviour from incompatible to compatible, that is $k_DREE^{Gt/L} = 1.0$, is related to atomic number. For example, Pertermann et al. (2004) report $k_DGd^{Gt/L} \sim 1.0$ and whereas McKenzie and O'Nions (1995) estimated and $k_DDy^{Gt/L} \sim 1.0$. It is clear from Fig. 11 that the potential crystallizing assemblage for the upper lavas must comprise approximately 59% Al-Cpx + 41% Gt to satisfy major element constraints. Using an estimate of $k_DDy^{Cpx/L} \sim 0.5$ (e.g., McKenzie and O'Nions, 1995; Pertermann et al., 2004) and $k_DDy^{Gt/L} \sim 1.7$ would give a bulk partition coefficient for this assemblage for Dy of ~1.

Additionally, because $k_DY^{Gt/L} > 1$ whereas $k_DZr^{Gt/L} << 1$ and $k_DSr^{Gt/L} << 1$, garnet crystallization would be expected to cause increasing Zr/Y and Sr/Y with decreasing MgO, a trend which is observed in the data (Fig. 11). Significantly, because plagioclase ($k_DSr^{Pl/L} \geq 1$; $k_DZr^{Pl/L} < 1$) is replaced by garnet at high pressure, magmas that have evolved by crystallization of garnet should have high Sr concentrations and high Sr/Y, a feature which is observed in the NWM upper lavas (Figs. 11b and 5d). By contrast, magmas within plagioclase on the liquidus will evolve to low Sr/Y and low Sr concentrations as is observed for the near 1 atm crystallization of the SLF and LSSC. Additionally, extensive low-pressure crystallization of Cpx, as exemplified by high Y plugs (Kerr et al., 1999) and Ben More trachyte, results in increasing in Zr/Y at <3 wt% MgO (Kerr and Thompson, 1995). The crystallization of the assemblage 59% Al-Cpx and 41% garnet is also a logical explanation for the behaviour of scandium in the NWM upper lavas (Fig. 5f) for which $k_DSc^{Gt/L} \sim 5$ (Le Roux et al., 2015). Fig. 12 illustrates the results of modelling of trace element profiles formed by fractional crystallization of a mixture of 59% Al-Cpx and 41% garnet from Cruach Sleibhe upper lava CS-JHP-1.13 containing 8.3 wt% MgO (Fig. 6c). Partition coefficients are taken from the compilation in Hole et al. (2023) and the proportions of Gt and

Table 1
Least-squares mixing model for Beinn Duill parent basalt (BD-JHP-1.16) to hawaiite (BD-JHP-1.14).

	SiO_2	TiO_2	Al_2O_3	FeO_T	MnO	MgO	CaO	Na_2O	K_2O	P_2O_5
BD-JHP-1.14	47.99	2.82	17.35	13.26	0.15	5.45	7.24	4.36	0.91	0.47
Cpx[1]	47.53	1.13	12.57	11.34	0.20	13.48	12.46	1.28	0.00	0.00
Garnet[1]	41.13	1.16	21.95	15.60	0.41	13.45	6.20	0.05	0.05	0.00
BD-JHP-1.16	46.50	2.12	16.88	13.50	0.19	8.34	8.65	2.75	0.86	0.22
Residuals:	-0.26	-0.04	-0.10	0.31	-0.02	-0.29	0.36	-0.19	0.30	-0.07

Sum of Squares of residuals 0.52. F=0.4 0.59Cpx 0.41Gt
[1] 2 GPa and Al-Cpx and Garnet compositions from the melting experiments of Thompson (1974).

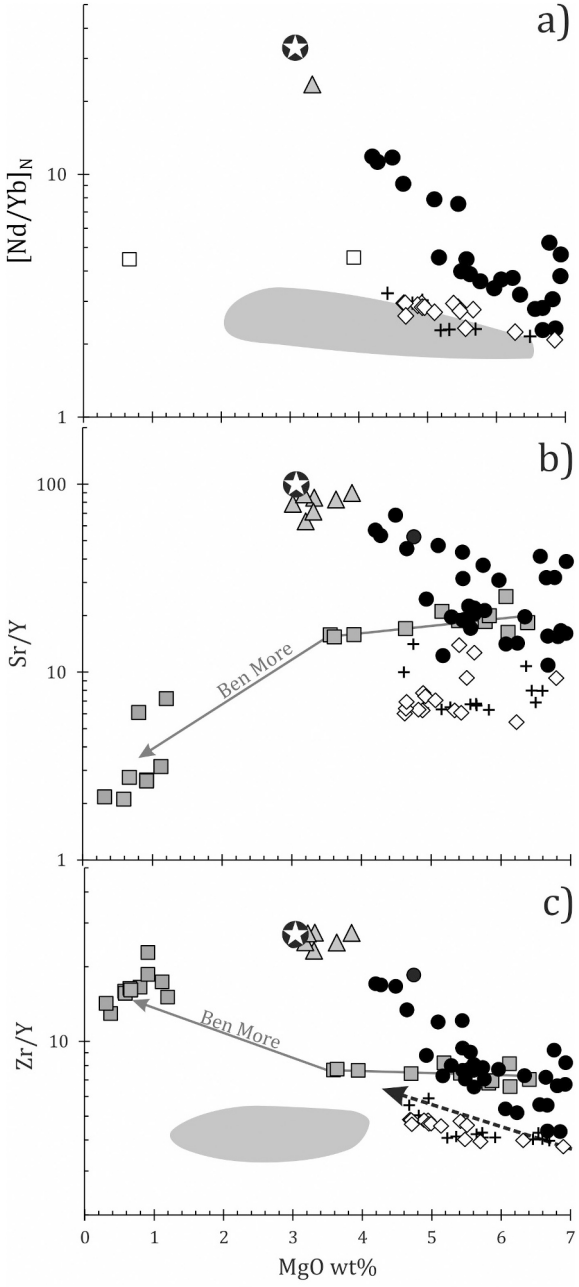

Fig. 11. Covariation between MgO (wt%) and a) Chondrite-normalized Nd/Yb ($[Nd/Yb]_N$); b) Sr/Y and c) Zr/Y for north Mull lavas LSSC and SLF. The trend for Ben More 'Pale Suite' lavas and other Mull trachytes is taken from Kerr et al. (1999). Symbols as for Fig. 9. The black pecked arrow in c) is the crystallization trend for Faroe Islands lower lavas from Bernstein (1994).

Al-Cpx are chosen so that the bulk partition coefficient for Dy~1 is as described above (see also supplementary information). Also shown are models for an assemblage of 59% Al-Cpx and 41% plagioclase which does not exhibit the HREE depletion caused by garnet, and predictably, develops a negative Sr anomaly compared to Pr and Nd. Such a pattern is like that for the most evolved Ben More mugearites and trachytes (e.g., BM66; Fig. 12) which fall on a low pressure cotectic (Fig. 9b). The crystallization of an extract of 59% Al-Cpx and 41% garnet from a basalt with ~8 wt% MgO can thus provide a satisfactory explanation for the observed trends in trace element abundances in the NWM upper lavas and the low Y mugearite.

5.6. Pyroxenite versus peridotite melting and magma mixing

Garnet is stable on the pyroxenite solidus to lower pressures than peridotite (~1.9 GPa; Kogiso et al., 2003; Lambart et al., 2016; Hole et al., 2023). Consequently, if pyroxenite was involved in the petrogenesis of the NW Mull lavas it might be possible for the observed REE fractionation to be a consequence of progressive melting of a garnet-pyroxenite source. Indeed, partial melting of eclogite at ~2 GPa can produce primary melts that are evolved (2.9–5.7 wt% MgO; Takahashi et al., 1998), but these are silica-saturated andesitic compositions (Herzberg, 2011; Takahashi et al., 1998) and are therefore unlike the Mull low Y mugearites. However, it is established that pyroxenite melts have quite different Zn/Fe and Zn/Mn from peridotite melts (e.g., Hole et al., 2023; Howarth and Harris, 2017; Zhang et al., 2021). Peridotite-derived melts have 10^4Zn/Fe in the range of 8.5–12.5 (Zhang et al., 2021) and Zn/Mn in the range 0.05–0.07 (Howarth and Harris, 2017) whereas pyroxenite-derived magmas exceed the maxima for peridotite-derived magmas. All but the most evolved NWM lavas fall well within the region for peridotite-derived magmas in terms of Zn/Fe (Fig. 13). Evolved SLF samples (<6 wt% MgO) have high Zn/Fe (10^4Zn/Fe up to 20) because DFe > DZn for clinopyroxene crystallization (Le Roux et al., 2015) and these lavas formed along the 1 atm Ol + Pl + Cpx cotectic. In terms of Zn/Mn, the same evolved SLF lavas, the low Y mugearite and some of the NWM upper lavas stray into the region for pyroxenite melts (Fig. 13; Zn/Mn > 0.07; Howarth and Harris, 2017) but this could be a consequence of garnet or Al-Cpx fractionation rather than a melting effect, because k_DZn < k_DMn in both garnet and Al-Cpx (e.g., Le Roux et al., 2015). Additionally, Hole (2018) noted that there is no evidence from trace elements in olivine phenocrysts for a contribution from pyroxenite melting in the Beinn Reudle lavas. We are therefore confident that any contribution from pyroxenite melting was minimal and that the observed REE fractionation was caused by fractional crystallization of Al-Cpx + Gt.

The REE profiles in Fig. 6 could be produced by mixing between a peridotite-derived basaltic magma and a low MgO melt generated from eclogite/pyroxenite. A key geochemical characteristic of mixing is the generation of near-linear covariations between MgO and major and incompatible trace elements (e.g., Meade et al., 2009; Troll et al., 2021) which is not a feature of the NWM lavas. Indeed, the NWM lavas describe curvilinear trends between MgO, Zr, Nb and La (Fig. 5) typical of the trends produced by fractional crystallization. We are therefore confident that the dominant magmatic process governing evolution of the NWM lavas was fractional crystallization, with additional concomitant assimilation of crust in the lower lavas.

5.7. Magmatic plumbing beneath NW Mull

NWM lower lavas show clear signs of interaction with continental crust (Figs. 7 and 8) whereas NWM upper lavas, with a garnet crystallization signature, exhibit little or no crustal signature. Consequently, to preserve the chemical fingerprint of garnet crystallization in lavas magma must have risen from deep lithospheric magma chambers without significant interaction with lithospheric mantle or continental crust and without pausing significantly before eruption.

NWM lower lavas are generally more MgO-rich and therefore hotter than the NWM upper lavas (Fig. 4). This leads us to propose that the magmatic plumbing system was such that the NWM lower lavas assimilated acidic partial melts of crust during ATA (Kerr et al., 1995) and insulated and lined magma conduits leading to the surface. The NWM upper lavas utilized these same conduits allowing them to avoid direct contact with fusible crustal components, and the fact that they were also cooler than the NWM lower lavas, reduced further the likelihood of contamination. These observations fit broadly with progressively inhibited crustal contamination, a process invoked in other parts of the NAIP (Meade et al., 2014). Whether this local reduction in crustal contamination with time resulted from an exhaustion of easily fusible

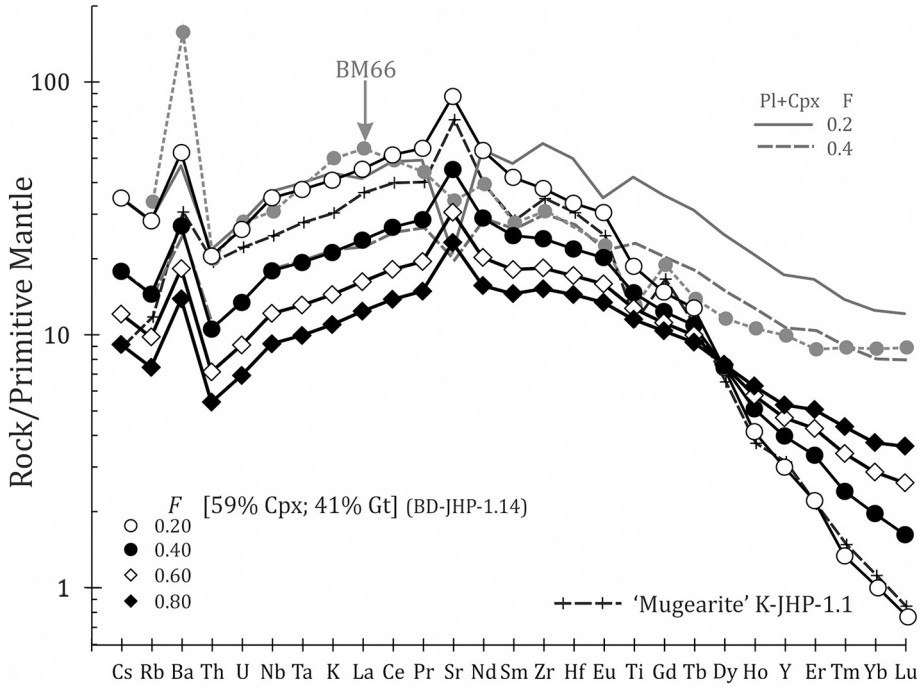

Fig. 12. a) Primitive mantle-normalized (Sun and McDonough, 1988) generated by fractional crystallization of an assemblage of 59% clinopyroxene and 41% garnet from starting composition CS-JHP-1.13. *F* refers to amount of liquid remaining in the system during crystallization. Partition coefficients for the REE in clinopyroxene and garnet are given in the supplementary materials. Low Y mugearite K-JHP-1.1 is shown for comparison. BM66 is a high Y trachyte from Ben More and the grey solid and pecked lines are model patterns replacing plagioclase with garnet for *F* indicated.

components (sensu Meade et al., 2014), or whether conduit lining by residual crystallized components of migrated melts protected the later melts, or some combination remains conjectural.

The local tectonic regime could also have influenced the petrogenesis of these lavas Indeed, Hole et al. (2015) highlighted the importance of tectonic controls on the distribution and composition of BPIP magmas which might related to an abrupt change from contractional deformation to stress relaxation in the adjacent European continent (Nielsen et al., 2007). Emplacement of the Staffa Lava Formation was related to synmagmatic normal faulting and graben formation (Jolley et al., 2009; Lyle, 2000; Williamson and Bell, 2012), with sediments and lava flows emplaced into two NW–SE trending fault-controlled valleys (Jolley et al., 2009). SLF flows are typically columnar jointed and ponded with pillow lavas at their base and are interbedded with alluvial and lacustrine sedimentary rocks which indicate an overall southeasterly drainage direction. The famous Fingal's Cave flow, which is approximately 50 m thick, is of this type. The interbedded sedimentary rocks frequently contain clasts derived from the underlying siliciclastic and chalky Mesozoic strata. A series of unconformities separates different members of the SLF, requiring periods of uplift subsidence and erosion during valley-fill (Williamson and Bell, 2012). This period of lithospheric stretching may therefore have facilitated storage and crystallization magmas close to the surface.

In contrast, NWM lavas are rarely ponded, pillow lavas are absent and interbedded sedimentary rocks are uncommon. Where sedimentary rocks do occur, (e.g. Calgary conglomerate) they are almost entirely made of locally-derived lava clasts and fine-grained tephra or are thin red-coloured tuffaceous deposits. These observations suggest that the NWM lava field was building topography and was not emplaced into a graben system. This potential change from an extensional to a passive or compressional tectonic regime appears to have been coincident with a change from shallow, low-pressure to deep, high-pressure storage and crystallization of magma before eruption.

Periods of extension and graben formation resulted in plumbing system that allowed magma storage close to the surface as in the case of the SLF. Subsequently, when extension ceased, shallow magma chambers were no longer accessible, possibly because the plumbing system remained full of crystallized or partly crystallized magma. A pathway to the surface for subsequent magmas that included their storage at low pressure, may not have been available. We therefore suggest that pressure of crystallization of Mull lavas is mainly controlled by local, and quite rapid, changes in tectonic regime.

As noted earlier, the preservation of identifiable geochemical signatures of garnet fractionation in lavas requires storage at ~2 GPa and eruption at the surface without pausing to equilibrate at lower pressure, and without interaction with the lithosphere. Additionally, a clear garnet signature only becomes evident in relatively evolved, cotectic magmas (<7 wt% MgO). Given that such a combination of factors is likely to be quite rare in natural systems, this is a sensible explanation as to why evidence for garnet fractionation is not widespread amongst LIPs. Indeed, cotectic compositions will only record the pressure of magma storage at which the cotectic was reached; deeper magma storage and crystallization will be overprinted by signatures of shallower crystallization (Herzberg, 2004; Morrison et al., 1985). We have investigated this using Petrolog3 for crystallization of a model primary magma in two sets of pressure steps (Fig. 9b), firstly 1.0 and 0.0 GPa and secondly, 1.4 and 0.0 GPa with 30% crystallization occurring at the higher pressure and the remainder at 0.0 GPa. In both cases, evolved liquids intersect the 0.0 GPa isobar in Fig. 9b, and this occurs at ~4.5 and 5.5 wt% MgO over the lower and higher-pressure intervals respectively. It is worthy of note that liquids on the steep parts of the polybaric curves towards lower pressures in Fig. 9b are all Ol + Pl + Cpx cotectics.

Bernstein (1994) argued that a positive covariation in Zr/Y (2.5–6.5) with MgO (4.5–7.7 wt%) in Faroes Islands Lower Lavas was the result of garnet fractionation at depth. However, inspection of Fig. 11 shows that over a similar range of MgO contents, the NWM lavas exhibit a far greater variability in Zr/Y (up to 20) than the Faroes lavas. Additionally, Millett et al. (2020) showed that the compositions of Beinisvørð Formation Lavas (stratigraphically equivalent to the lower basalts of Bernstein, 1994) with 4.5–7.0 wt% MgO were consistent with

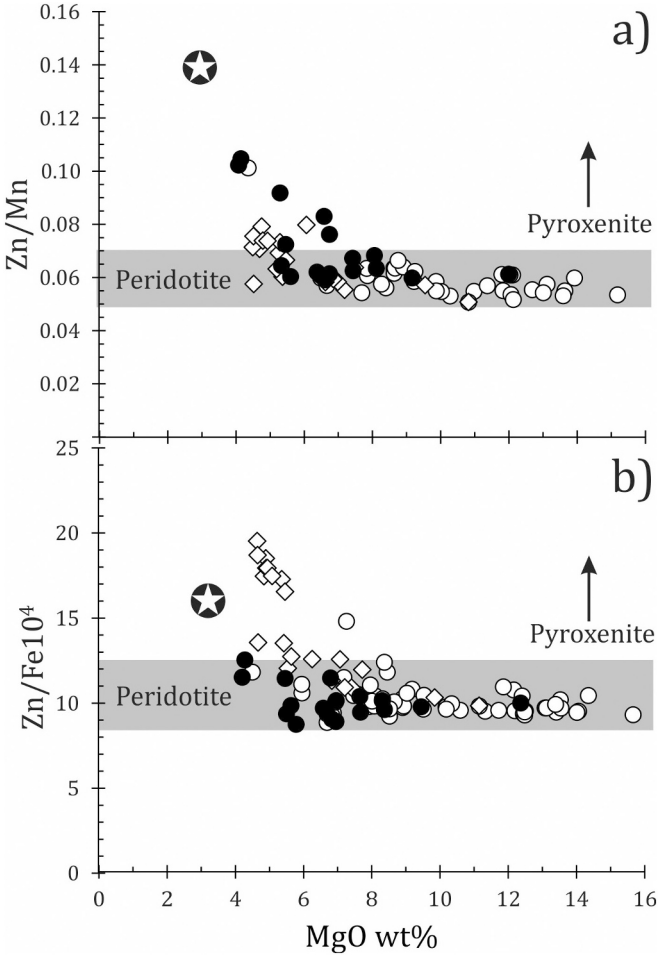

Fig. 13. Zn/Mn and Zn/Fe•10^4 versus MgO (wt%) for NWM and SLF lavas. The horizontal grey shading represents the regions for peridotite-derived melts and are taken from Zhang et al. (2021) and Howarth and Harris (2017). Pyroxenite melts will plot above these fields.

crystallization at 0.3 ± 0.1GPa. We therefore conclude that garnet fractionation was unlikely to have occurred in the Faroes Islands lavas.

We conclude that uncontaminated peridotite-derived lavas that have undergone garnet fractionation are extremely rare and require a specific set of circumstances to be preserved, not least of which is transport of magma directly from the site of crystallization to the surface without pause. In the case of Hawaii, Yang et al. (2023) propose that melts that had fractionated garnet re-equilibrate with harzburgite at <2 GPa and it is unlikely that this multistage melting process will preserve a garnet signature in erupted compositions.

6. Conclusions

1) The lava field of northwest Mull is subdivided based on geochemical compositions into basal, lower and upper suites. Basal lavas are hawaiites (~6 wt% MgO), lower lavas are picrite-basalt (16–8 wt% MgO) and upper lavas are mostly hawaiite (3–8 wt% MgO).
2) Lower lavas exhibit key trace element ratios (e.g., La/Ta, Th/Ta) that are consistent with interaction between a mantle peridotite-derived melt with sialic crustal materials. Conversely, upper lavas lack any significant signature of crustal contamination and represent a consanguineous series related by fractional crystallization alone.
3) Progressively inhibited crustal contamination resulted in the lower lavas removing fusible portions of the crust and assimilating them. Upper lavas avoided significant crustal contamination because they used the same magma conduits as the lower lavas and avoided contact with fusible crust.
4) Major element projections in the system Di-An-En and CS-A-MS require pressure of fractional crystallization >1.4 GPa for upper lavas with cotectic composition (<7 wt% MgO). These are consistent with pressure estimates by other workers using a variety of methodologies (e.g., Hole, 2018; Liu and Presnall, 2000; Thompson, 1974). Examination of the system CS-A-MS shows that upper lavas evolved by fractional crystallization of Al-Cpx → Pl or Al-Cpx → Gt, with garnet replacing Al-Cpx at pressure > 1.8 GPa.
5) Increasing LREE-enrichment and HREE-depletion with decreasing MgO ($[Nd/Yb]_N$ ~ 2 at 7 wt% MgO to 32 at 3 wt% MgO), high Sr/Y (up to 100), high absolute Sr abundances (>1100) and high Zr/Y (up to 27) suggest garnet was a fractionating phase during evolution of the upper lavas. Modelling of major and trace elements suggests an assemblage of 59% Al-Cpx and 41% garnet could produce the observed compositional variation in the upper lavas.
6) Periods of extension and graben formation during the emplacement of the low pressure SLF, resulted in plumbing system that allowed magma storage close to the surface. Subsequently, when extension ceased shallow magma chambers were no longer accessible, possibly because the plumbing system remained full of crystallized or partly crystallized magma. Subsequent magmas therefore could not access the shallow storage areas in the crust and crystallized at depth.
7) Preservation of a garnet signature in lavas of LIPs requires a very specific set of circumstances. In most cases, polybaric crystallization effectively erases any signature of very high-pressure processes.

Declaration of Competing Interest

The authors declare that they have no known competing financial interests or personal relationships that could have appeared to influence the work reported in this paper.

Acknowledgements

We thank Jussi Heinonen and an anonymous reviewer for a constructive and thoughtful criticism. We thank James Westland for pointing us at useful and interesting localities on the Isle of Mull. This study was part funded by a University of Aberdeen Elphinstone Scholarship to JHP.

Appendix A. Supplementary data

Supplementary data to this article can be found online at https://doi.org/10.1016/j.lithos.2023.107397.

References

Beckinsale, R.D., Pankhurst, R.J., Skelhorn, R.R., Walsh, J.N., 1978. Geochemistry and petrogenesis of the early Tertiary lava pile of the Isle of Mull, Scotland. Contrib. Mineral. Petrol. 66, 415–427.
Bernstein, S., 1994. High-pressure fractionation in rift-related basaltic magmatism: Faeroe plateau basalts. Geology 22, 815–818.
Danyushevsky, L.V., 2001. The effect of small amounts of H_2O on crystallization of mid-ocean ridge and back-arc basin magmas. J. Volcanol. Geotherm. Res. 110, 265–280.
Danyushevsky, L.V., Plechov, P., 2011. Petrolog3: integrated software for modeling crystallization processes. Geochem. Geophys. Geosyst. 12 https://doi.org/10.1029/2011GC003516.
DePaolo, D.J., 1981. Trace element and isotope effects of combined wall rock assimilation and fractional crystallization. Earth Planet. Sci. Lett. 53, 189–202.
Dickin, A.P., Jones, N.W., Thirlwall, M.F., Thompson, R.N., 1987. A Ce/Nd isotope study of crustal contamination processes affecting Paleocene magmas in Skye, Northwest Scotland. Contrib. Mineral. Petrol. 96, 455–464.
Fram, M.S., Lesher, C.E., 1997. Generation and polybaric differentiation of East Greenland early Tertiary flood basalts. J. Petrol. 38, 231–275.
Herzberg, C., 2004. Partial crystallization of mid-ocean ridge basalts in the crust and mantle. J. Petrol. 45, 2389–2405.
Herzberg, C., 2011. Identification of source lithology in the Hawaiian and Canary Islands: implications for origins. J. Petrol. 52, 113–146.

Herzberg, C., Asimow, P.D., 2015. PRIMELT3 MEGA.XLSM software for primary magma calculation: peridotite primary magma MgO contents from the liquidus to the solidus. Geochem. Geophys. Geosyst. 16, 563–578.
Herzberg, C., O'Hara, M.J., 2002. Plume-associated ultramafic magmas of Phanerozoic age. J. Petrol. 43, 1857–1883.
Hole, M.J., 2018. Mineralogical and geochemical evidence for polybaric fractional crystallization of continental flood basalts and implications for identification of peridotite and pyroxenite source lithologies. Earth Sci. Rev. 176, 51–67.
Hole, M.J., Millett, J.M., 2016. Controls of mantle potential temperature and lithospheric thickness on magmatism in the North Atlantic Igneous Province. J. Petrol. 57, 417–436.
Hole, M.J., Millett, J.M., Rogers, N.W., Jolley, D.W., 2015. Rifting and mafic magmatism in the Hebridean basins. J. Geol. Soc. Lond. 172, 218–236.
Hole, M.J., Gibson, S.A., Morris, M.C., 2023. Slab window–related magmatism as a probe for pyroxenite heterogeneities in the upper mantle. Geology 51, 268–272.
Howarth, G.H., Harris, C., 2017. Discriminating between pyroxenite and peridotite sources for continental flood basalts (CFB) in southern Africa using olivine chemistry. Earth Planet. Sci. Lett. 475, 143–151.
Johnson, D.M., Hooper, P.R., Conrey, R.M., 1999. XRF analysis of rocks and minerals for major and trace elements on a single low dilution li-tetraborate fused bead. Adv. X-ray Anal. 41, 843–867.
Jolley, D.W., Bell, B.R., Williamson, I.T., Prince, I., 2009. Syn-eruption vegetation dynamics, paleosurfaces and structural controls on lava field vegetation: an example from the Palaeogene Staffa Formation, Mull Lava Field, Scotland. Rev. Palaeobot. Palynol. 153, 19–33.
Jolley, D.W., Millett, J.M., Schofield, N., Broadley, L., Hole, M.J., 2021. Stratigraphy of volcanic rock successions of the North Atlantic rifted margin: the offshore record of the Faroe–Shetland and Rockall basins. Earth Environ. Trans. R. Soc. Edinb. 1–28.
Kent, R.W., Thomson, B.A., Skelhorn, R.A., Kerr, A.C., Norry, M.J., Walsh, J.N., 1998. Emplacement of Hebridean Tertiary flood basalts: evidence from an inflated pahoehoe lava flow on Mull, Scotland. J. Geol. Soc. Lond. 155, 599–607.
Kerr, A.C., 1998. On the nature of the parental magma of the Palaeogene Staff Magma sub-type, Isle of Mull, Scotland. Trans. R. Soc. Edinb. Earth Sci. 89, 87–93.
Kerr, A.C., Thompson, R.N., 1995. High-pressure fractionation in rift-related basaltic magmatism: Faeroe plateau basalts. Comment. Geology 23, 671–672.
Kerr, A.C., Kempton, P.D., Thompson, R.N., 1995. Crustal assimilation during turbulent magma ascent (ATA); new isotopic evidence from the Mull Tertiary lava succession, N. W. Scotland. Contrib. Mineral. Petrol. 119, 142–154.
Kerr, A.C., Kent, R.W., Thomson, B.A., Seedhouse, J.K., Donaldson, C.H., 1999. Geochemical evolution of the Tertiary Mull Volcano, Western Scotland. J. Petrol. 40, 873–908.
Knaack, C., Cornelius, S.B., Hooper, P.R., . Trace Element Analyses of Rocks and Minerals by ICP-MS. GeoAnalytical Lab. http://www.wsu.edu/%E2%88%BCgeolab/note/icpms.html. Washington State University.
Kogiso, T., Hirschmann, M.M., Frost, D.J., 2003. High-pressure partial melting of garnet pyroxenite: possible mafic lithologies in the source of ocean island basalts. Earth Planet. Sci. Lett. 216, 603–617.
Kress, V.C., Carmichael, I.S.E., 1988. Stoichiometry of the iron oxidation reaction in silicate melt. Am. Mineral. 73, 1267–1274.
Lambart, S., Baker, M.B., Stopler, E.M., 2016. The role of pyroxenite in basalt genesis: Melt-PX, a melting parameterization for mantle pyroxenites between 0.9 and 5GPa. J. Geophys. Res. https://doi.org/10.1002/2015JB012762.
Le Maitre, R.W., Streckeisen, A., Zanettin, B., Le Bas, M.J., Bonin, B., Bateman, P., Bellieni, B., Dudek, A., Efremova, S., Keller, J., Lamere, J., Sabine, P.A., Schmid, R., Sorensen, H., Woolley, A.R., 2002. Igneous Rocks: A Classification and Glossary of Terms, Recommendations of the International Union of Geological Sciences, Subcommission of the Systematics of Igneous Rocks. Cambridge University Press.
Le Roux, V., Dasgupta, R., Lee, C.-T.A., 2015. Recommended mineral-melt partition coefficients for FRTEs (Cu), Ga, and Ge during mantle melting. Am. Mineral. 100, 2533–2544.
Liu, T.-C., Presnall, D.C., 2000. Liquidus phase relations in the system $CaO–MgO–Al_2O_3–SiO_2$ at 2·0 GPa: applications to basalt fractionation, eclogites, and igneous sapphirine. J. Petrol. 41, 3–20.
Lyle, P., 2000. The eruptive environment of multi-tiered columnar basalt flows. J. Geol. Soc. Lond. 157, 715–722.
Matzen, A.K., Baker, M.B., Beckett, J.R., Wood, B.J., 2017. The effect of liquid composition on the partitioning of Ni between olivine and silicate melt. Contrib. Mineral. Petrol. 172.
McKenzie, D.P., O'Nions, R.K., 1995. The source region of Ocean Island basalts. J. Petrol. 36, 133–159.
Meade, F.C., Chew, D.M., Troll, V.R., Ellam, R.M., Page, L.M., 2009. Magma ascent along a major Terrane boundary: crustal contamination and magma mixing at the drumadoon intrusive complex, Isle of Arran, Scotland. J. Petrol. 12, 2345–2374.
Meade, F.C., Troll, V.R., Ellam, R.M., Freda, C., Font, L., Donaldson, C.H., Klonowska, I., 2014. Bimodal magmatism produced by progressively inhibited crustal assimilation. Nat. Commun. 5, 4199.
Milholland, C.S., Presnall, D.C., 1998. Liquidus phase relations in the $CaO–MgO–Al_2O_3–SiO_2$ system at 3·0 GPa: the aluminous pyroxene thermal divide and high-pressure fractionation of picritic and komatiitic magmas. J. Petrol. 39, 3–27.
Millett, J.M., Hole, M.J., Jolley, D.W., Passey, S.R., Rossetti, L., 2020. Transient mantle cooling linked to regional volcanic shut-down and early rifting in the North Atlantic Igneous Province. Bull. Volcanol. 2020, 61–82.
Morrison, M.A., Thompson, R.N., Dickin, A.P., 1985. Geochemical evidence for complex magmatic plumbing during development of a continental volcanic centre. Geology 13, 581–584.
Nevaskil, H., Dondolini, A., Horn, J., Filiberto, J., Lonh, H., Lindsey, D.H., 2004. The origin and evolution of silica-saturated Alkalic suites: an experimental study. J. Petrol. 45, 693–721.
Nielsen, S.B., Stephenson, R.A., Thomsen, E., 2007. Dynamics of Mid-Palaeocene North Atlantic rifting linked with European intra-plate deformations. Nature 450, 1071–1074.
O'Hara, M.J., 1968. The bearing of phase equilibria studies in synthetic and natural systems on the origin and evolution of basic and ultrabasic rocks. Earth Sci. Rev. 4, 69–133.
Pertermann, M., Hirschmann, M.M., Hametner, K., Gunther, D., Schmidt, M.W., 2004. Experimental determination of trace element partitioning between garnet and silica-rich liquid during anhydrous partial melting of MORB-like eclogite. Geochem. Geophys. Geosyst. 5, 1–23.
Preston, R.J., Bell, B.R., Rogers, G., 1998. The Loch Scridain Xenolithic Sill complex, Isle of Mull, Scotland: fractional crystallization, assimilation, magma-mixing and crustal anatexis in subvolcanic conduits. J. Petrol. 39, 519–550.
Pugsley, J.H., 2021. The Stratigraphic Architecture and Evolution of the North-West Mull Lava Field, Isle of Mull, Scotland. Unpublished PhD thesis. University of Aberdeen.
Putirka, K.D., 2008. Thermometers and barometers for volcanic systems. Rev. Mineral. Petrol. 69, 61–120.
Sugarawa, T., 2000. Empirical relationships between temperature, pressure, and MgO content in olivine and pyroxene saturated liquid. J. Geophys. Res. B4, 8457–8472.
Sun, S.-S., McDonough, W.F., 1988. Chemical and isotopic systematics of oceanic basalts: implications for mantle composition and processes. In: Saunders, A.D., Norry, M.J. (Eds.), Magmatism in the ocean basins. Geological Society, 42. Special Publications, London, pp. 313–345.
Takahashi, E., Nakajima, K., Wright, T.L., 1998. Origin of the Columbia River basalts: melting model of a heterogeneous plume head. Earth Planet. Sci. Lett. 162, 63–80.
Thompson, R.N., 1974. Primary basalts and magma genesis I: Skye, North-West Scotland. Contrib. Mineral. Petrol. 45, 317–341.
Thompson, R.N., 1982. Magmatism in the British Tertiary volcanic province. Scott. J. Geol. 18, 49–107.
Thompson, R.N., Gibson, I.L., Marriner, G.F., Mattey, D.P., Morrison, M.A., 1980. Trace element evidence of multistage mantle fusion and polybaric fractional crystallisation in the Palaeocene lavas of Skye, NW Scotland. J. Petrol. 21, 265–293.
Thompson, R.N., Dickin, A.P., Gibson, I.L., Morrison, M.A., 1982. Elemental fingerprints of isotopic contamination of Hebridean Palaeocene mantle-derived magmas by Archaean Sial. Contrib. Mineral. Petrol. 79, 159–168.
Thompson, R.N., Morrison, M.A., Dickin, A.P., Gibson, I.L., Harmon, R.S., 1986. Two contrasting styles of interaction between basic magmas and continental crust in the British Tertiary Volcanic Province. J. Geophys. Res. 91, 5985–5997.
Troll, V.R., Nicoll, G.R., Ellam, R.M., Emeleus, C.H., Mattsson, T., 2021. Petrogenesis of the Loch Bà ring-dyke and Centre 3 granites, Isle of Mull, Scotland. Contrib. Mineral. Petrol. 176, 16.
Villiger, S., Ulmer, P., Muntener, O., Thompson, B., 2004. The liquid line of descent of anhydrous, mantle-derived, tholeiitic liquids by fractional and equilibrium crystallization—an experimental study at 1.0 GPa. J. Petrol. 45, 2369–2388.
Villiger, S., Ulmer, P., Muntener, O., 2007. Equilibrium and fractional crystallization experiments at 0.7 GPa; the effect of pressure on phase relations and liquid compositions of tholeiitic magmas. J. Petrol. 48, 159–184.
Whitaker, M.L., Nekvasil, H., Lindsley, D.H., Difrancesco, N.J., 2007. The role of pressure in producing compositional diversity in intraplate basaltic magmas. J. Petrol. 48, 365–393.
Williamson, I.T., Bell, B.R., 1994. The Palaeocene lava field of west-Central Skye, Scotland: stratigraphy, palaeogeography and structure. Trans. R. Soc. Edinb. Earth Sci. 85, 39–75.
Williamson, I.T., Bell, B.R., 2012. The Staffa Lava formation: graben related volcanism, associated sedimentation and landscape character during the early development of the Palaeogene Mull Lava Field, NW Scotland. Scott. J. Geol. 48, 1–46.
Yang, H.-J., Kinzler, R.J., Grove, T.L., 1996. Experiments and models of anhydrous, basaltic olivine-plagioclase-augite saturated melts from 0.001 to 10 kbar. Contrib. Mineral. Petrol. 124, 1–18.
Yang, J., Wang, C., Zhang, W., Zhenmin, J., 2023. Genesis of Hawaiian lavas by crystallization of picritic magma in the deep mantle. Nat. Commun. 14, 1382.
Zhang, Y., Sun, C.Y.M., Huang, Z., Narantsetseg, T., Ren, Z., Li, P., Zhang, Q., 2021. Contrasting compositions between phenocrystic and xenocrystic olivines in the Cenozoic basalts from Central Mongolia: constraints on source lithology and regional uplift. Am. Mineral. 106, 251–264.